Nitrogen Physisorption on Defective C_{60}

Juan M. D. Tascón

Instituto Nacional del Carbón, CSIC, Apartado 73, 33080 Oviedo, Spain

Eduardo J. Bottani*

Instituto de Investigaciones Fisicoquímicas Teóricas y Aplicadas, (UNLP-CIC-CONICET), Casilla de Correo 16, Sucursal 4, (1900) La Plata, Argentina

Received: February 7, 2002; In Final Form: April 22, 2002

Nitrogen physical adsorption, from 50 up to 120 K, on a defective C_{60} fullerene solid is studied with Grand Canonical Monte Carlo computer simulations. New adsorption sites are produced due to the creation of a vacancy in the fcc crystal structure of C_{60}. The distributions of molecules with respect to their gas−solid and gas−gas interaction energies are analyzed. The contribution of the internal cavity of the solid to the total surface area is estimated from the local isotherms. The adsorbate cross-sectional area is calculated at all temperatures. The isosteric heat of adsorption is calculated from the Henry's Law constant. The adsorption energy distribution functions are discussed comparing the simulation results with experimental isotherms.

Introduction

The discovery, more than one decade ago, of the fullerene structure[1,2] brought about the first type of molecular solids consisting exclusively of carbon. In this structure, carbon atoms cluster in polyhedral aggregates, the best-known ones being C_{60} (pseudospherical) and C_{70} (ellipsoidal). In turn, these carbon polyhedra arrange in the solid state in crystalline structures, e.g., a face-centered cubic (fcc) one for C_{60}.[3]

It is well-known that, upon thermobaric treatment, the fcc structure of C_{60}, stable at ambient conditions, changes first to a number of fcc lattices with decreased parameters and later to more distorted structures and even amorphous phases. Dramatic changes in the mechanical properties (e.g., hardness) of C_{60} and other fullerenes have stimulated a great deal of research on the structural transformations of these materials upon pressure/temperature treatments.[4−9]

Structural defects play an important role in the structural transformations in fullerenes. Thus, dislocations in C_{60} crystals have been suggested to promote polymerization of C_{60} molecules in crystals.[10] Some features of order−disorder phase transitions in C_{60} near 260 K have been associated with the presence of stacking faults.[11,12] Therefore, understanding the structure and properties of fullerenes requires a detailed characterization of structural defects, as already pointed out in the pioneering work by Fischer et al.[13]

Like other physicochemical properties, the adsorption behavior of fullerenes can be expected to depend on the structural features of this type of material. In previous works from our laboratories,[14,15] physical adsorption of simple gases (N_2, Ar, CO_2) on high-purity, well-crystallized C_{60} has been experimentally measured and compared with results of computer simulations. A good agreement was obtained between both types of results confirming the validity of the model and its parameters. The experimental data obtained using different techniques and the simulation results are consistent with the existence of several adsorption centers. Those centers have been assigned for the surface of the fcc lattice, namely: (i) on top of C_{60} molecules, (ii) located in "channels" between two C_{60} molecules, and (iii,) located at places where four C_{60} molecules meet. Therefore, occurrence of structural defects such as vacancies of C_{60} molecules from the fcc structure will affect the adsorption properties of these solids. In this work we have thought of interest to study the influence of structural defects on the adsorption properties of these solids. To this end, we have simulated N_2 adsorption isotherms on a model surface of crystalline C_{60} where fullerene spheres have been eliminated to create vacancies in the crystal structure.

In this paper we will describe nitrogen adsorption on C_{60} solid with defects in the crystal structure. A wide temperature range has been studied starting at 50 K up to 120 K. The simulated adsorption isotherm at 77.5 K is compared with experimental results previously published. The adsorption energy distribution function is analyzed and related to topographic characteristics of the model solid. The isosteric heat of adsorption has been calculated from the Henry's law constant. Microdensity profiles together with several distributions are employed to describe how nitrogen adsorption progresses as the number of adsorbed molecules increases. The local adsorption isotherms are also calculated together with the density of the adsorbed phase on different parts of the surface. The average cross-sectional area of nitrogen molecule is calculated at all the temperatures studied.

Technical Details

The Monte Carlo method has been employed to perform the simulations reported here using the Grand Canonical Ensemble. The simulations are carried out at constant chemical potential (μ), volume (V), and temperature (T), and the average value of a given property (X) is given by:

$$\langle X\rangle_{\mu VT} = \Xi^{-1}\sum_{N=0}^{\infty}\frac{V^N z^N}{N!}\int\cdots\int X(\mathbf{q})\exp[-\beta U_N(\mathbf{q})]\,d\mathbf{q} \quad (1)$$

* Author to whom correspondence should be addressed. Tel: 54-221-425-7430. Fax: 54-221-425-4642. E-mail: ebottani@inifta.unlp.edu.ar.

10.1021/jp020368d CCC: $22.00
Published on Web 08/23/2002

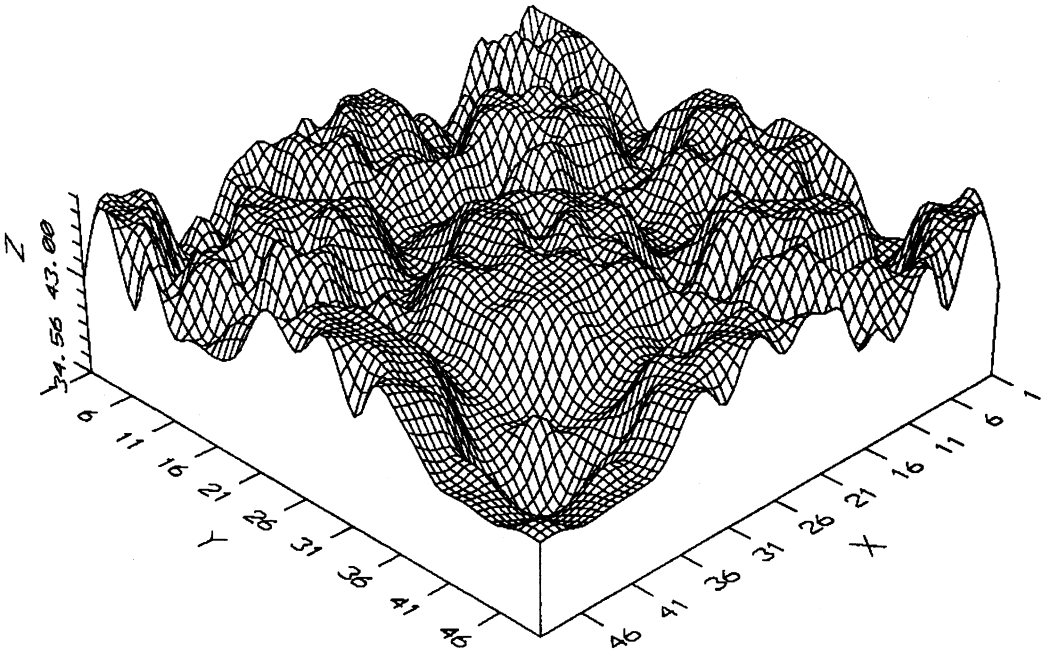

Figure 1. Topographic map of the model solid with one vacancy created by deleting one C_{60} molecule in each unit cell. The units in *x* and *y* directions are arbitrary and *z* is in Å.

where $\beta = 1/kT$, k is the Boltzmann's constant, $\mathbf{q}$ is the set of molecular coordinates, Ξ is the grand partition function, z is the activity given by $z = \exp(\beta\mu)/\Lambda^3$, $\Lambda = h^2/(2\pi mkT)^{1/2}$, and $U_N(\mathbf{q})$ is the total potential energy of a given configuration that includes the energies of interaction between adsorbed molecules and the solid and between pairs of adsorbed molecules. The integrals in eq 1 are evaluated following the Monte Carlo method using the following transition probabilities:

$$\min\left\{1,\left[\frac{zV}{N+1}\right]\exp[-\beta(U_{N+1}-U_N)]\right\} \tag{2}$$

for a creation step, where z is the activity of the adsorbate and N is the number of adsorbed molecules, and

$$\min\left\{1,\left[\frac{N}{zV}\right]\exp[-\beta(U_{N+1}-U_N)]\right\} \tag{3}$$

for a destruction step, and

$$\min\{1, \exp[-\beta(U_{N,i}-U_{N,j})]\} \tag{4}$$

for a molecular displacement attempt which includes translation and rotation movements. More details on the algorithm have been previously published.[15]

The structure of the solid employed consists of C_{60} molecules arranged to form a face-centered cubic structure with one vacancy in one face of the unit cell. The simulation box contains 140 C_{60} molecules and its geometric area is 8.03 nm^2. Periodic boundary conditions were applied in both *x* and *y* directions to generate an infinite surface and to avoid border effects. All distances in the *z* direction are measured from the bottom of the simulation box that is considered as the reference plane. The density of the solid (1.4 g/cm^3) is smaller than the real solid density (1.82 g/cm^3) due to the created defects. C_{60} molecules are considered as a collection of 60 spherical Lennard−Jones interaction sites located on the coordinates of carbon atoms of each C_{60} molecule. Also C_{60} molecules are modeled as rigid bodies.

The energy of the adsorbed molecules is calculated as the sum of gas−solid and gas−gas energies, both calculated with Lennard−Jones functions. The pairwise summation approximation is employed. The interaction parameters employed in this work are the same as in a previous paper.[14] The potentials chosen to describe the interactions should be regarded as effective pair potentials. Nevertheless it has been proved that it is possible to obtain reasonable descriptions of many systems via computer simulation.[16] The interaction energy between adsorbed molecules includes dispersion and electrostatic contributions. The model adsorbate consists of two Lennard−Jones interaction sites located on each nitrogen atom separated at a distance of 0.110 nm. To simulate the quadrupole moment of a nitrogen molecule[17] three discrete electrical charges are employed: two located on each nitrogen atom (-6.49×10^{-20} C) and one positive charge (12.98×10^{-20} C) located on the symmetry center of the molecule.[17] This charge distribution reproduces the experimental value of the quadrupole moment. Each simulation point was calculated from 7.2×10^9 configurations except the first point of each run to which 2.2×10^{10} configurations were generated. For simulations at 63 and 77.5 K the acceptance ratio of movements and creation/destruction of molecules were kept approximately equal to 40−50% and 1−3%, respectively. With the same set of parameters the acceptance ratio for movements increased to 60% for the simulations at 120 K and decreased to 25−30% for the simulations at 50 K. To improve the statistics the length of the simulation has been increased with respect to previous work.[14,15] The first point of each simulation run starts with a "clean" surface and adsorbate molecules are randomly created or destroyed with probabilities given by eqs 2 and 3. This is the reason the first point needs more simulation steps to reach equilibrium. The following points are simulated using the last configuration generated for the previous one.

Results and Discussion

Figure 1 shows a 3D map of the surface as detected by a nitrogen molecule adsorbed on the surface. To obtain this plot a molecule is placed on the surface and its energy minimized

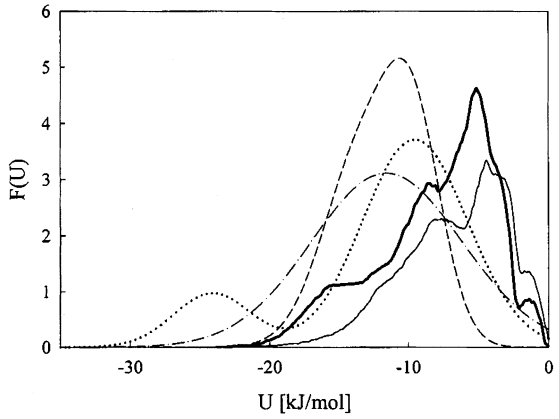

Figure 2. Adsorption energy (U) distributions ($F(U)$) obtained from the energy maps of the perfect fcc solid (thicker line) and the defective solid (thinner line). The other distributions have been obtained from the adsorption isotherms: (●) from ref 19, (- - -) simulation at 120 K, and, (−♦−♦−) simulation at 77.5 K.

TABLE 1: Parameters Obtained from the Deconvolution of the Adsorption Energy Distribution Corresponding to the Defective Surface and Shown in Figure 2[a]

peak	amplitude	center [kJ/mol]	width
1	0.370	-11.86 ± 0.08	1.31 ± 0.09
2	1.214	-7.66 ± 0.06	1.84 ± 0.09
3	1.102	-7.1 ± 0.4	4.7 ± 0.2
4	2.083	-4.31 ± 0.02	0.83 ± 0.02
5	1.645	-2.86 ± 0.01	0.54 ± 0.01
6	0.816	-1.24 ± 0.01	0.52 ± 0.04

[a] For the perfect surface the obtained peaks are centered at: −13.9, −9.1, and −5.0 kJ/mol.[14]

with respect to its vertical distance to the surface. Once the minimum energy is achieved the molecular mass center Z coordinate is recorded. This process is repeated for all points of an arbitrarily chosen mesh. In our case a 50 × 50 mesh has been employed. The first characteristic of the obtained map is that it is not symmetrical as was the case for the perfect crystal (see Figure 7 in ref 14). The creation of one vacancy in the unit cell produces minor changes in the shape of the adsorption energy distribution with respect to the perfect solid (see Figure 2 thicker and thinner full lines). The distribution corresponding to the defective surface can be decomposed into six Gaussian peaks instead of three peaks obtained for the perfect solid. Table 1 summarizes the main characteristics of those peaks which can be assigned to adsorption sites by comparison with the perfect solid results. Thus, the peak located at ca. −11 kJ/mol in the distribution of the defective solid corresponds to sites of type A (space between four C_{60} molecules). Peaks 2 and 3 can be associated to sites B (space between two C_{60} molecules), and the fourth peak quoted in Table 1 corresponds to adsorption on top of C_{60} molecules (site C). The two last peaks (5 and 6) correspond to new adsorption sites located in the region where the vacancy has been created. The small shift of the peaks with respect to the perfect crystal could be due to the lack of symmetry of the adsorption potential.

Numerical simulations allow the calculation of the total potential energy of the adsorbed molecules and its dependency on the number of adsorbed molecules. The profiles obtained at all the temperatures studied are shown in Figure 3 and compared with the perfect solid profile. At temperatures between 50 and 77.5 K the energy of the adsorbed phase on the defective solid is always larger than in the perfect one, which has been obtained at 77.5 K. At 120 K the behavior is reversed probably due to the larger kinetic energy of the adsorbed molecules or an

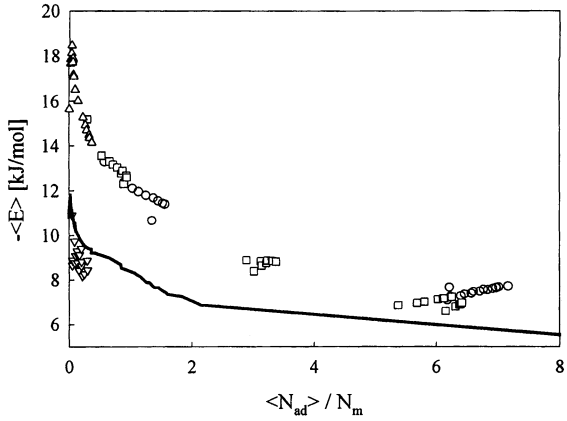

Figure 3. Average total potential energy ($\langle -E \rangle$) at different temperatures for the defective (symbols) and perfect solid (full line) as a function of surface coverage. $\langle N_{ad} \rangle$ is the average number of adsorbed molecules and N_m is the BET monolayer capacity. $T = 50$ K (○), 63 K (□), 77.5 K (Δ), and 120 K (∇).

unrealistic value of the monolayer capacity, N_m, employed. We will further discuss this point in more detail. Notwithstanding the difference in absolute values, the profiles obtained for both solids have the same shape and are characteristic of heterogeneous surfaces. The isosteric heat of adsorption extrapolated to zero coverage has been calculated using the following expression:[18]

$$Q_{st}(0) = R\left(\frac{\partial \ln K_h}{\partial 1/T}\right) \tag{5}$$

where K_h is the Henry's Law constant. The obtained value for the defective solid is larger (21.5 kJ/mol) than the one obtained for the perfect solid (15.4 kJ/mol),[14] and both values are larger than the accepted value for nitrogen adsorption on the basal plane of graphite (ca. 10 kJ/mol).

Another effect due to existence of a vacancy is the obvious increase in the exposed surface of the solid. The experimental isotherm obtained in our laboratory using a well-purified and crystallized sample has been showed in a previous paper[14] thus it is not included here. Our simulation on the perfect solid reproduced the experimental results as has been also shown elsewhere.[14]

The specific surface area of the sample employed in ref 19 is larger (ca. 7 m^2/g) than the one of our sample (0.3 m^2/g). This is not unexpected because the main impurities present in Ismail's samples could be C_{70} and soot that normally tend to increase the surface area. In our simulations on the defective solid, the vacancy created increases the BET surface area from 11.63 nm^2 for the perfect solid to 19.20 nm^2. Both values have been obtained from the simulated isotherms of nitrogen at 77.5 K. The isotherms obtained from the simulations are compared with the experimental one in Figure 4. As could be expected, all fall on the same curve because all the solids are of the same chemical nature mainly showing differences in their surface area.

The peaks observed in the microdensity profiles (see Figure 5) obtained at different temperatures and approximately the same surface coverage (ca. 0.25 monolayers) show that most of the adsorption sites are accessible at 50 K as well as at 120 K. At 120 K, nitrogen adsorption on the external part of the solid ($z/\sigma > 12 \pm 0.5$) is larger than at 50 K. This can be explained by the higher thermal kinetic energy of the adsorbate at 120 K. The profiles obtained at 63 and 77.5 K exhibit the same peaks as the 50 K profile. The small differences in the height of the peaks for temperatures between 50 and 77.5 K are due to the

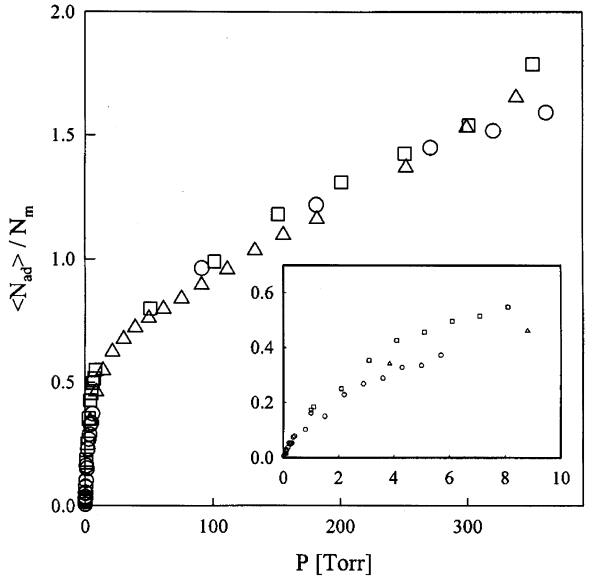

Figure 4. Nitrogen adsorption isotherms at 77.5 K. Simulations with the defective solid (○), and the perfect fcc solid (□). The experimental isotherm (Δ) has been obtained from ref 17. The inset corresponds to the very low pressure region.

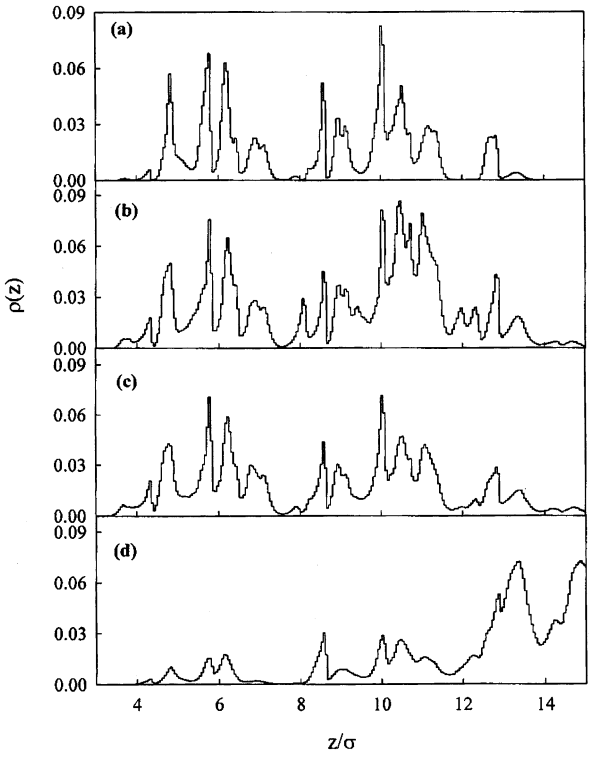

Figure 5. Microdensity, $\rho(z)$, profiles obtained at 50 K (a), 63 K (b), 77.5 K (c), and 120 K (d) as a function of the distance from the bottom of the simulation box, z. σ is the gas−gas distance parameter = 0.332 nm.

fact that all the profiles have not been obtained at exactly the same number of adsorbed molecules.

The distributions of molecules with respect to their gas−solid interaction energy show that the adsorbed molecules are able to detect the most energetic sites at temperatures below 77.5 K (panels a and b in Figure 6). Those sites are located below the surface between the C_{60} molecules in agreement with previous simulations of nitrogen adsorption on a perfect crystalline solid.[14] These profiles also show that at low temperatures the

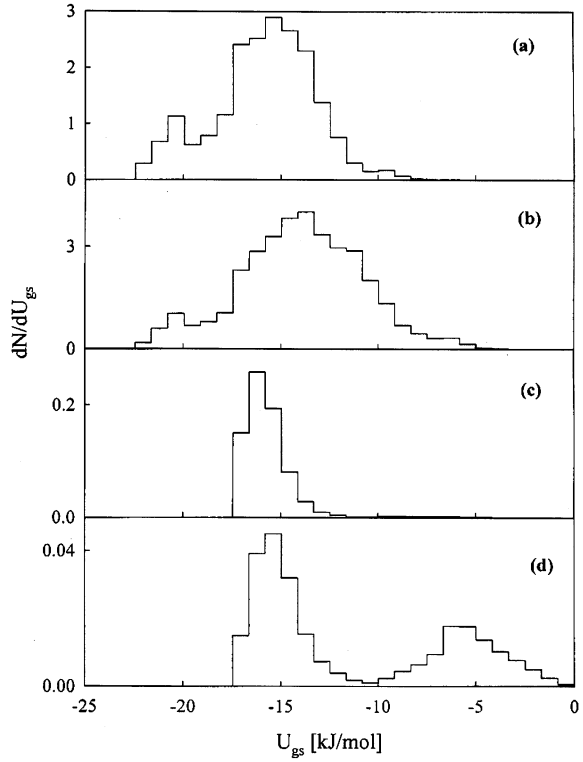

Figure 6. Distributions of adsorbed molecules with respect the gas−solid energy (U_{gs}) obtained at 50 K (a), 63 K (b), 77.5 K (c), and 120 K (d). All the profiles have been obtained at approximately the same number of adsorbed molecules.

adsorbed molecules have not enough kinetic energy to abandon the most energetic sites.

In Figure 2 the adsorption energy distribution functions obtained from the isotherms are also included. Those distributions have been calculated using the method described elsewhere.[20] The distribution functions obtained from the energy maps agree with the distributions of molecules with respect to their gas−solid energy (Figure 6). The distributions obtained from the simulated adsorption isotherms represent an average of the true ones (calculated from the energy maps).

The main difference between the distributions obtained at 77.5 and 120 K is that the last one is a double Gaussian with peaks located at −13.2 and −9.5 kJ/mol. It must be pointed out that those peaks are in the same position of the peaks corresponding to sites A and B in the perfect solid that are also present in the defective one. The distribution obtained from Ismail's experimental isotherm has two peaks, one located at −24.1 kJ/mol and the other at −9.5 kJ/mol. The last one is in agreement with the results obtained from the simulations presented here and previous results.[14,15] The second peak located at higher energies could be confirming the presence of impurities already mentioned.

The distributions obtained at 77.5 and 120 K reproduce the simulated isotherms as well as the BET monolayer capacity. At 77.5 K the calculated monolayer capacity differs in less than 1% with respect to the BET value while at 120 K this difference is ca. 4%. This result also confirms the value of the monolayer capacity at 120 K and the difference in the total energy profiles should be ascribed to other effects.

The microdensity profiles (Figure 5) and the distributions of molecules with respect to their gas−solid energy (Figure 6) show that at high temperatures the adsorbate does not get trapped in the cavities below the surface plane formed by the top of the C_{60} molecules even though they are accessible.

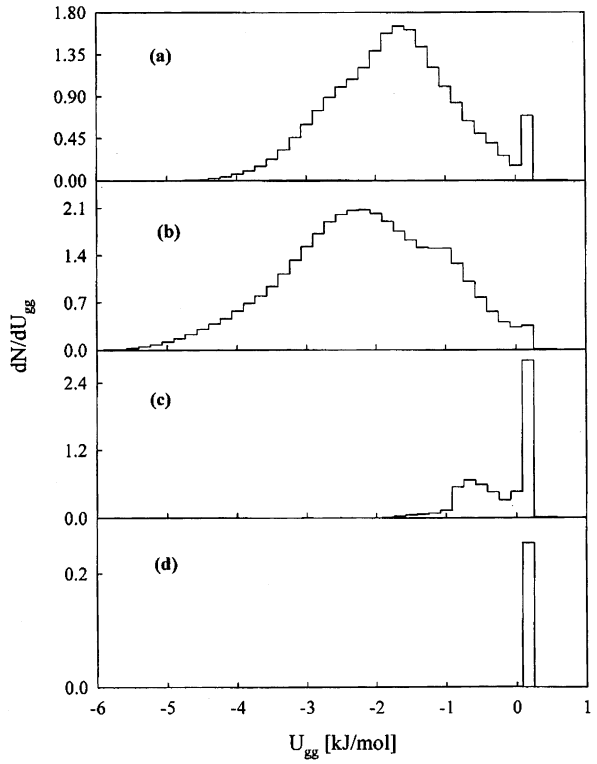

Figure 7. Distributions of adsorbed molecules with respect to the gas−gas interaction energy (U_{gg}) obtained at 50 K (a), 63 K (b), 77.5 K (c), and 120 K (d). All but the 77.5 K profiles have been obtained at approximately the same surface coverage.

The distributions of molecules with respect to the gas−gas interaction energy (Figure 7) obtained at submonolayer coverage indicate that at 120 K repulsive interactions are predominant, while at 63 and 50 K attractive energies are found for most of the molecules. At 77.5 K an intermediate situation is found, moreover the profile shown in Figure 7c has been obtained for a larger number of adsorbed molecules in order to obtain a noticeable proportion of molecules experiencing attractive interactions. The position of the attractive energy peak at 77.5 K is consistent with the minimum of the interaction potential for a pair of nitrogen molecules with their molecular axis parallel to each other (−1.2 kJ/mol at a separation distance of 0.34 nm). At 50 and 63 K the maximum of the distributions is shifted toward larger energies.

The microdensity profiles can be integrated to calculate the densities of the adsorbed film in arbitrary chosen portions of the adsorption space. The relative densities with respect to the solid and liquid nitrogen bulk phases have been calculated in the region below the surface plane. Taking the solid phase as reference at 50 K the calculated relative density is 1.1 ± 0.2, while at 63 K and taking the liquid as reference the relative density is 0.9 ± 0.1. At 77.5 K and in the same surface coverage range, the relative density with respect to the liquid is 0.6 ± 0.1. At larger equilibrium pressures nitrogen tends to be in a liquidlike state as has been reported in a previous study.[15]

The local adsorption isotherms are very similar to the ones determined for the perfect solid. The BET surface area obtained from the local adsorption isotherms indicates that ca. 59% of the specific area is due to the cavities and the vacancy. In the case of the perfect solid the contribution of the cavities constitutes ca. 28% of the total area of the solid. The 50 K local adsorption isotherm corresponding to the adsorption on the external surface produces a BET area equal to the geometric area of the simulation box (8.03 nm^2) suggesting that the multilayer formed on the external surface is almost flat and uniform.

TABLE 2: Nitrogen Cross-Sectional Area Obtained Averaging All the Configurations Generated in the Simulations

T [K]	$\langle\sigma\rangle$ [nm^2]
120.0	0.172 ± 0.018
77.5	0.158 ± 0.013
63.0	0.158 ± 0.009
50.0	0.163 ± 0.009

The average cross-sectional area of the adsorbate has been obtained using all the configurations generated. The obtained values are quoted in Table 2. The value obtained at 77.5 K is almost equal to the one previously obtained for the adsorption on the perfect solid (0.154 ± 0.001 nm^2). Nevertheless the values of the cross-sectional area corresponding to each surface coverage exhibit larger fluctuations with respect to the results obtained for the perfect solid. It is not possible to elaborate a complete explanation of those fluctuations. The cross-sectional area obtained at 77.5 K is 0.150 nm^2 when the number of adsorbed molecules corresponds to a monolayer and the surface covered is 20.8 nm^2, which is very close to the BET value (19.2 nm^2).

As a final remark it must be pointed out that the results obtained from our simulations are in agreement with conclusions derived from other experimental results. As examples, it can be mentioned IR data for the adsorption of CO and nitrogen oxide obtained by Fastow et al.[21,22] and the ones published by Papirer et al.[23] using inverse gas chromatography to compare the adsorption of organic vapors on graphite, carbon black, and fullerene (C_{60}) samples. It must be also said that the idea of modeling a solid and then simulating the adsorption of different probes as a validation of the model has been recently employed by Bakaev et al. to study the structure of glass surfaces.[24,25]

Conclusions

The agreement between the experimental data to which our simulations are compared and conclusions derived from other experiments confirm the model employed for the simulations and also the validity of the parameters of the interaction potentials. Nitrogen physisorption on a perfect crystalline C_{60} solid shows the same general characteristics as the same gas adsorbed on a defective solid. The main differences can be explained through the increase in the surface area due to the vacancies generated and to the more heterogeneous character of the defective solid surface. As could be expected the isosteric heat of adsorption extrapolated at zero coverage is larger on the defective solid than on the perfect fcc crystal. In the defective solid ca. 59% of the total area is below the surface plane. At all temperatures studied nitrogen molecules can access all the cavities. At 50 K the adsorbate is in solidlike phase as can be inferred from the calculated density. At 63 and 77.5 K the density is close to the density of pure liquid nitrogen. According to the BET surface area obtained from the local isotherms, at 50 K the external surface is covered with a flat uniform nitrogen layer. Nitrogen cross-sectional area is within the accepted values and the fluctuations observed as the surface coverage increases could be due to the heterogeneous character of the solid. The simulations also show that the BET monolayer capacity is a good estimate of this magnitude.

Acknowledgment. E.J.B. is Associate Professor of the National University of "El Litoral" and researcher of the Comisión de Investigaciones Científicas de la Provincia de

Buenos Aires. The Spanish team acknowledges financial support from CICYT (Project 1FD1997-1915) and DGICYT (Project PB98-0492).

References and Notes

(1) Kroto, H. W.; Heath, J. R.; O'Brien, S. C.; Curl, R. F.; Smalley, R. E. *Nature* **1985**, *318*, 162.
(2) Krätschmer, W.; Lamb, L. D.; Fostiropoulos, K.; Huffman, D. R. *Nature* **1990**, *347*, 354.
(3) Dresselhaus, M. S.; Dresselhaus, G.; Eklund, P. C. In *Science of Fullerenes and Carbon Nanotubes*; Academic Press: San Diego, 1996; Chapter 7, pp 171−223.
(4) Davydov, V. A.; Kashevarova, L. S.; Rakhmanina, A. V.; Agafonov, V.; Céolin, R.; Szwarc, H. *Carbon* **1997**, *35*, 735.
(5) Blank, V. D.; Buga, S. G.; Dubitsky, G. A.; Serebryanaya, N. R.; Popov, M. Yu.; Sundqvist, B. *Carbon* **1998**, *36*, 319.
(6) Hirai, H. *New Diamond Frontier Carbon Technol.* **2000**, *10*, 313.
(7) Liu, Z. G.; Ohi, H.; Masuyama, K.; Tsuchiya, K.; Umemoto, M. *J. Mater. Res.* **2000**, *15*, 1528.
(8) Blank, V. D.; Kulnitskiy, B. A.; Zhigalina, O. M. *Carbon* **2000**, *38*, 2051.
(9) Serebryanaya, N. R.; Blank, V. D.; Ivdenko, V. A.; Chernozatonskii, L. A. *Solid State Commun.* **2001**, *118*, 183.
(10) Dyachenko-Dekov, D. V.; Iunin, Y. L.; Iztozov, A. N.; Kveder, V. V.; Nikolaev, R. K.; Orlov, V. I.; Ossipyan, Y. A.; Sidorov, N. S.; Steinman, E. A. *Phys. Status Solidi B* **2000**, *222*, 111.
(11) Lubenets, S. V.; Natsik, V. D.; Fomenko, L. S.; Isakina, A. P.; Prokhvatilov, A. I.; Strzhemechny, M. A.; Aksenova, N. A.; Ruoff, R. S. *Low Temp Phys.* **1997**, *23*, 251.
(12) Gu, M.; Tang, T. B.; Yan, F.; Feng, D. *Chin. Phys. Lett.* **1998**, *15*, 357.
(13) Fischer, J. E.; Heiney, P.; Luzzi, D. E.; Cox, D. E. In *Fullerenes. Synthesis, Properties and Chemistry of Large Carbon Clusters*; Hammond, G. S., Kuck, V. J., Eds.; ACS Symp. Ser. 481, 1992; Chapter 4, p 55.
(14) Martínez-Alonso, A.; Tascón, J. M. D.; Bottani, E. J. *Langmuir* **2000**, *16*, 1343.
(15) Martínez-Alonso, A.; Tascón, J. M. D.; Bottani, E. J. *J. Phys. Chem. B* **2001**, *105*, 135.
(16) Allen, M. P.; Tildesley, D. J. In *Computer Simulation of Liquids*; Oxford Science Publishing, 1991.
(17) Bottani, E. J. *Langmuir* **2001**, *17*, 2733.
(18) Cascarini de Torre, L. E.; Flores, E. S.; Llanos, J. L.; Bottani, E. J. *Langmuir* **1995**, *11*, 4742.
(19) Ismail, M. K. I.; Rodgers, S. L. *Carbon* **1992**, *30*, 229.
(20) Cascarini de Torre, L. E.; Bottani, E. J. *Colloids Surf. A* **1996**, *116*, 285.
(21) Fastow, M.; Kozirovski, Y.; Folman, K.; Heidberg, J. *J. Phys. Chem.* **1992**, *96*, 6126.
(22) Fastow, M.; Kozirovski, Y.; Folman, K. *Surf. Sci.* **1995**, *331*, 121.
(23) Papirer, E.; Breudle, E.; Ozil, F.; Balard, H. *Carbon* **1999**, *37*, 1265.
(24) Bakaev, V. A.; Steele, W. A. *J. Chem. Phys.* **1999**, *111*, 98.
(25) Bakaev, V. A.; Steele, W. A.; Bakaeva, T. I.; Pantano, C. G. *J. Chem. Phys.* **1999**, *111*, 9813.